Available online at www.sciencedirect.com
SCIENCE DIRECT
Journal of Colloid and Interface Science 286 (2005) 670–680
JOURNAL OF Colloid and Interface Science
www.elsevier.com/locate/jcis

A robust algorithm for the simultaneous parameter estimation of interfacial tension and contact angle from sessile drop profiles

Nicole M. Dingle, Michael T. Harris *

School of Chemical Engineering, Forney Hall of Chemical Engineering, Purdue University, West Lafayette, IN 47907, USA

Received 25 October 2004; accepted 21 January 2005

Available online 19 February 2005

Abstract

The pendant and sessile drop profile analysis using the finite element method (PSDA-FEM) is an algorithm which allows simultaneous determination of the interfacial tension (γ) and contact angle (θ_c) from sessile drop profiles. The PSDA-FEM algorithm solves the nonlinear second-order spherical coordinate form of the Young–Laplace equation. Thus, the boundary conditions at the drop apex and contact position of the drop with the substrate are required to solve for the drop profile coordinates. The boundary condition at the position where the drop contacts the substrate may be specified as a fixed contact line or fixed contact angle. This paper will focus on the fixed contact angle boundary condition for sessile drops on a substrate and how this boundary condition is used in the PSDA-FEM curve-fitting algorithm. The PSDA-FEM algorithm has been tested using simulated drop shapes with and without the addition of random error to the drop profile coordinates. The random error is varied to simulate the effect of camera resolution on the estimates of γ and θ_c values obtained from the curve-fitting algorithm. The error in the experimental values for γ from sessile drops of water on acrylic and Mazola corn oil on acrylic falls within the predicted range of errors obtained for γ values from simulated sessile drop profiles with randomized errors that are comparable in magnitude to the resolution of the experimental setup.

Keywords: Sessile drop; Interfacial tension; Contact angle; Finite element method

1. Introduction

Liquids wet solids in various areas of natural and industrial processes. An understanding of the wetting behavior of a liquid on a substrate is useful during adsorption phenomena, crystallization processes, coating applications, drug discovery, and oil recovery [1–7]. The contact angle is a parameter that illustrates the wetting characteristic of a liquid on a substrate or medium. Solid surface properties are also obtained from contact angle measurements by solving Young's equation. This equation is derived from a force balance of three line tensions: the liquid–vapor (γ_{LV}), the solid–liquid (γ_{SL}), and the solid–vapor (γ_{SV}) for a liquid drop resting on a substrate expressed as

$$\cos\theta_c = \frac{\gamma_{SL} - \gamma_{SV}}{\gamma_{LV}}. \tag{1}$$

Contact angle measurements are performed using the Wilhelmy plate method [8,9], capillary rise method [10], thin fibers [2–11], a traditional goniometer with manual tangent placement, and the extraction of drop profile coordinates using a digital image. A manual contact goniometer is a simple and less sophisticated contact angle apparatus. This method uses a protractor to align a tangent along the three-phase contact point to determine the contact angle of liquid/solid systems. The error associated with using this instrument is $\pm 3°$, and varies based on user expertise [12]. Bateni et al. introduce the automated polynomial fit (APF) algorithm, a method similar to the goniometer method in that no fluid properties are necessary; however, the variability based on different users is removed [12]. The APF method

* Corresponding author. Fax: +1-765-494-0805.
E-mail address: mtharris@purdue.edu (M.T. Harris).

0021-9797/$ – see front matter
doi:10.1016/j.jcis.2005.01.087

uses magnified drop images, and does not use the governing equation to solve for the interfacial tension and contact angle. Therefore, the contact angle is obtained from a tangent placed at the three-phase contact point using a third-order polynomial fit.

Several techniques have been developed using the assumption that the sessile drop is spherical and gravitation effects are negligible [13,14]. The spherical cap assumption is limited to sessile drops with a small β (shape factor) or liquids with relatively high surface tension. Ying et al. propose a method to correct $\theta/2$ angle with a study of three different approaches (two different sessile drops, manual height and contact diameter, and intersection) [14]. The contact angle must be less than 90° with a drop of small volume for valid use of the spherical cap approximation. Chatterjee [15] discusses the limitations of the spherical cap approximation and its applications to highly spherical drop shapes.

The digitization of a drop profile along with numerical integration of the Young–Laplace equation to compute the best fit curve is a versatile, repeatable, accurate and widely used technique for determining the interfacial tension and contact angle of experimental systems [16–19]. Skinner et al. [20] and Moy et al. [21] develop a method based on the axisymmetric drop shape analysis of pendant and sessile drop profiles which requires an input of several system parameters. The surface tension, drop volume and equatorial diameter are necessary to initiate the algorithm. Huh and Reed [22] have also proposed the estimation of γ and θ_c from sessile drop profiles, however, only drops which contain an equatorial diameter can be used for their numerical technique.

Emelyanenko and co-workers [23] review the effect of video discretization on the accuracy of pendant and sessile drop experiments. More recently, Cabezas et al. [24] present a new drop shape method which fits theoretical gradient images to experimental images to overcome the problem of edge detection where optical or experimental limitations distort the digital profile. The resolution and optical performance of the camera used in drop shape image analysis affect the accuracy and reproducibility of reported experimental contact angle and interfacial tension values.

The initial work of Rotenberg et al. using ADSA-P (axisymmetric drop shape analysis-profile) has been updated by several other members of the Neumann research group [12]. The ADSA-CD [20] calculates the contact angle for systems with low contact angles (less than 20°) and is suitable for biological systems or nonhomogeneous surfaces. A top view of the drop is used to obtain the contact diameter experimentally and use it as an input parameter in the algorithm. This differs from the widely used techniques requiring a side view of the drop profile to obtain the contact angle, and was further modified to ADSA-MD [21] and both algorithms were combined and automated in ADSA-D (diameter) [25]. The ADSA-CD numerical algorithm is also very useful in the estimation of the contact angle for drops that are not perfectly axisymmetric and when the substrate is rough. The angle limitation for ADSA-CD and ADSA-MD is that the contact angle must be less than 90°; however, ADSA-D is more universal and has no limit for applicable contact angles. It is important to note that the interfacial tension of the liquid drop must either be known or determined after calculating the contact angle of the system, or vice versa using ADSA-P.

A detailed overview of a novel algorithm γ-PD-FEM which utilizes a Galerkin/finite-element-based derivation in the spherical coordinate form of the Y–L equation to determine γ from pendant drop profiles has been accepted for publication by Dingle et al. [26]. The Y–L equation is a second-order differential equation; therefore, two boundary conditions are required to obtain the theoretical drop profile. These are the physical boundary conditions of the drop system which include the drop apex and the contact line where the drop attaches to the nozzle. The γ-PD-FEM algorithm solves the Y–L equation to obtain the theoretical pendant drop profile by imposing the axisymmetric boundary conditions at the apex of the drop and the "fixed contact line" boundary condition where the drop attaches to the nozzle. This eliminates the need to use arbitrary upper limits of integration.

Many of the current methods use shooting methods to determine the interfacial tension from pendant drop profiles and to solve the Young–Laplace equation expressed as three arc-length-based differential equations. Del Rio et al. report recent advancements in the ADSA program to solve for the Laplacian shape using finite difference along with collocation methods, which require one boundary condition at the apex [27]. ADSA-HD (height–diameter) requires that a second condition is defined and varies depending on the drop configuration (i.e., $\theta_c < 90°$ or $\theta_c < 90°$) for the boundary value problem. The contact angle (θ_c) estimates are calculated by back-substitution into three arc-length-based differential equations after determination of the estimate for β.

In this work, the Galerkin/finite element method is used to solve for the surface function coordinates. The pendant and sessile drop analysis using the finite element method (PSDA-FEM) differs from other techniques because, like γ-PD-FEM, it requires physical boundary conditions at the drop apex and at the contact line to generate the theoretical drop profile. However, PSDA-FEM differs from γ-PD-FEM since the Y–L equation is solved by imposing the "fixed contact angle" boundary condition where the drop contacts the substrate.

The Galerkin/finite element method is used to solve the dimensionless Young–Laplace equation

$$-2\mathbf{H} = K \pm GY, \tag{2}$$

where the dimensionless parameters are the mean curvature, $\mathbf{H}$, the gravitational Bond number, G, the reference pressure, K, and Y is the axial coordinate defined further in Section 3.2. The negative sign is used for pendant drops, and the positive sign corresponds to sessile drops for the frame

of reference where y is positive in the direction opposite to gravity.

The PSDA-FEM algorithm in this research can simultaneously obtain parameter estimates for θ_c and γ without a priori knowledge of the interfacial tension by solving the second-order spherical coordinate form of the Y–L equation to generate the theoretical drop profile. This allows for studies of adsorption, mass transfer, and contamination of pure liquids by the substrate or by surface active agents on the substrate. This paper will discuss the FEM-based algorithm for obtaining parameter estimates for γ and the θ_c values when θ_c values are greater than, equal to, or less than 90°. The experimental apparatus and materials are summarized in Section 3. Simulated and experimental sessile drops of varying contact angles, volumes, and Bond numbers will be presented in Section 4. The interfacial tension values for experimental systems will be compared to results that are obtained from the pendant drop technique. The precision and accuracy of interfacial tension and contact angle parameter estimates that are obtained using the PSDA-FEM algorithm will also be presented to show the effect of camera resolution or video digitization on the parameter estimates.

2. Theoretical formulation

2.1. Spherical coordinate system

The equations used in the PSDA-FEM algorithm are formulated by first considering an axisymmetric pendant and sessile drop of density ρ_L suspended from or sitting on a substrate with a contact line of radius R, surrounded by a continuous fluid phase of density ρ_F, as shown in Fig. 1. The drop shape is expressed in spherical coordinates with the origin at the drop apex as $\mathbf{x}_{LF} = f(\theta)\mathbf{e}_r$, where $\mathbf{x}_{LF}$ is a dimensionless vector of interface location, f is the surface function, θ is the meridional angle measured from the axis of symmetry, and $\mathbf{e}_r$ and $\mathbf{e}_y$ are the unit vectors in the radial and axial direction, respectively [14].

A sessile drop shape is governed by the dimensionless Young–Laplace equation (2) on the surface of the liquid–fluid interface, S_{LF}. The characteristic length, drop radius (R), is used to define the dimensionless variables

$$\mathbf{H} = R\tilde{\mathbf{H}}, \qquad Y = \frac{\tilde{y}}{R}, \qquad K = \frac{\Delta p_0 R}{\gamma},$$
$$G = \frac{\Delta\rho g R^2}{\gamma}. \tag{3}$$

$2\mathbf{H}$ is twice the mean curvature of the interface (written in terms of the dimensional curvature, $\tilde{\mathbf{H}}$) and is defined as the negative of the surface divergence of the normal to the liquid–fluid interface (n_{LF}), i.e., $2\mathbf{H} = -\nabla_s \cdot n_{LF}$. Y is the axial coordinate where the dimensional distance from the contact line to the drop apex is defined as $\tilde{y}$. K is the reference pressure at the apex ($\tilde{y} = \tilde{y}_{max}$) of the drop for Δp_0 defined as the pressure difference at a selected datum plane, and G is the gravitational Bond number. The reference pressure, K, is calculated by placing a constraint on the drop volume (Vol). This volume is calculated in terms of the surface function coordinates:

$$\text{Vol} = \frac{2\pi}{3}\int_0^{\pi/2} f^3 \sin\theta \, d\theta. \tag{4}$$

The Y–L equation is used to solve for the theoretical drop profile coordinates subject to the boundary conditions

$$f_\theta = 0 \quad \text{at } \theta = 0, \tag{5a}$$
$$f = \text{contact radius} \quad \text{at } \theta = \pi/2, \tag{5b}$$
$$f_\theta = \sqrt{f^2 + f_\theta^2}\cos\theta_c \quad \text{at } \theta = \pi/2. \tag{5c}$$

Equation (5a) occurs at the apex and specifies that the drop is axially symmetric, and at $\theta = \pi/2$ the surface function

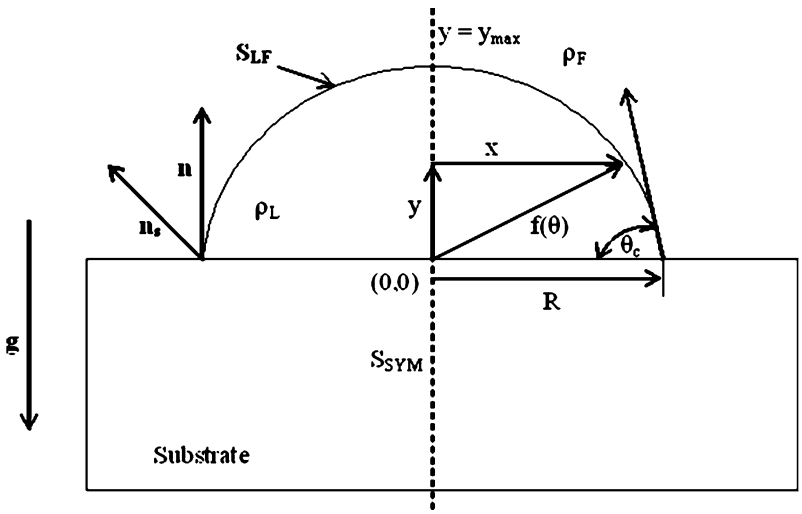

Fig. 1. Definition of the sessile drop spherical coordinate system used in PSDA-FEM algorithm.

equals the radius of the experimental drop for the fixed contact line condition (5b). The fixed contact angle boundary condition is expressed in terms of the derivative of f with respect to θ ($\mathrm{d}f/\mathrm{d}\theta = f_\theta$) which is written in terms of the contact angle shown in Eq. (5c).

2.2. G/FEM residual equations

The free drop shape is interpolated as

$$f(\theta) = \sum_{i=1}^{S} f_i \phi^i(\theta), \tag{6}$$

where the coefficients f_i are the nodal values of the drop free surface (theoretical coordinate points), $\mathbf{f} = (f_1, f_2, \ldots, f_S)$ is the vector of all the values, S is the total number of free surface nodes, ϕ^i is an appropriate basis function, and θ is the independent variable.

The Galerkin weighted residuals (R_i^{YL}) are formed by weighting the governing equation (2) by each weighting function ϕ^i and integrating the product over the drop surface,

$$R_i^{\mathrm{YL}} = \int_{S_{\mathrm{LF}}} \left[-2\mathbf{H} - (K + GY)\right]\phi^i e_r \cdot n_{\mathrm{LF}}\,\mathrm{d}S_{\mathrm{LF}} = 0, \quad i = 1, \ldots, S, \tag{7}$$

where there are S Young–Laplace residual equations ($R_1^{\mathrm{YL}}, \ldots, R_S^{\mathrm{YL}}$), which is equal to the number of free surface coordinates in Eq. (6). The mean curvature can be expressed in terms of $f(\theta)$, and the resulting expression is integrated by parts using the surface divergence theorem and is simplified by means of the boundary conditions (5). These steps yield

$$R_i^{\mathrm{YL}} = \int_0^{\pi/2} \left[\frac{f f_\theta \phi_\theta^i + \phi^i (2f^2 + f_\theta^2)}{\sqrt{f^2 + f_\theta^2}} - (K + Gf\cos\theta)\phi^i f^2 \right] \sin\theta\,\mathrm{d}\theta - f\phi^i \cos\theta_{\mathrm{c}}\Big|_{\theta=\pi/2} = 0, \quad i = 1, \ldots, S. \tag{8}$$

The final term in Eq. (8) arises from Young's equation where the contact angle is written in terms of the surface function coordinates. This is performed by computing the scalar product of the normal to the surface of the drop at the contact line (n) and the normal to the solid substrate (n_{s}). The expression for the contact angle is given by the equation

$$n \cdot n_{\mathrm{s}} = \cos\theta_{\mathrm{c}} = \frac{f_\theta}{\sqrt{f^2 + f_\theta^2}} \tag{9}$$

and is shown in the schematic of Fig. 1.

The integral in Eq. (8) is evaluated for all surface function values from 0 to $\pi/2$. The contact angle (θ_{c}) is incorporated at the final node when $\theta = \pi/2$. In contrast to the arc-length-dependent equations for which θ_{c} is obtained after back-substitution of the estimated γ value, the fixed contact angle boundary condition is incorporated into the residual Young–Laplace equation and allows the gravitation Bond number (from which the surface/interfacial tension is computed) and contact angle to be used simultaneously as fitting parameters.

3. Materials and method

3.1. Sample preparation

Sessile drop measurements were performed using distilled water and Mazola commercial brand vegetable cooking oil. A 1 × 1 cm cut microscope glass slide with acrylic tape (McMaster-Carr Supply Co.) adhered on the surface was selected as the solid substrate. Each sessile drop measurement was performed on the same substrate after the substrate had been cleaned and allowed to dry before the next measurement.

3.2. Pendant and sessile drop apparatus

A block diagram of the experimental apparatus developed for the sessile drop interfacial tension and contact angle measurements is shown in Fig. 2. The aluminum temperature chamber was designed and manufactured at Purdue University (Purdue Central Machine Shop). The chamber is also used to obtain pendant drop images for surface or interfacial tension measurements that were discussed in a previous paper [26]. In the current configuration, a 0.025 cm o.d. stainless steel needle is adjusted vertically by a smooth rack and pinion post holder. The needle is manually lowered into the environmental chamber.

A set volume of liquid is formed at a rate of 0.03 ml/min by the attached dual-syringe infusion/withdrawal pump (Cole Palmer/EW-74901-00). The liquid is placed on a 1 × 1 cm substrate which sits on a 4 × 1 × 1 cm aluminum block inside the environmental chamber. A sessile drop is formed by raising the nozzle using the rack and pinion post holder as the liquid flows from the nozzle tip. The temperature can be controlled to ±1 °C by two Thermatech HT type peltier (36 W) with fan accessories purchased from Melcor Inc. A Watech monochrome CCD camera with a 764 H × 494 V resolution captures the drop image, and the camera's signal is digitized by an IMAQ-NI-1407 image acquisition board (National Instrument Inc.) that is housed in an IBM compatible computer with a Pentium 4 processor. The entire apparatus is mounted on a vibration isolation table (Newport RS 4000), thus minimizing the error due to building vibrations.

In order to lessen the effect of interference rings, or multiple edges of the drop images, a Newport Inc. fiber optic

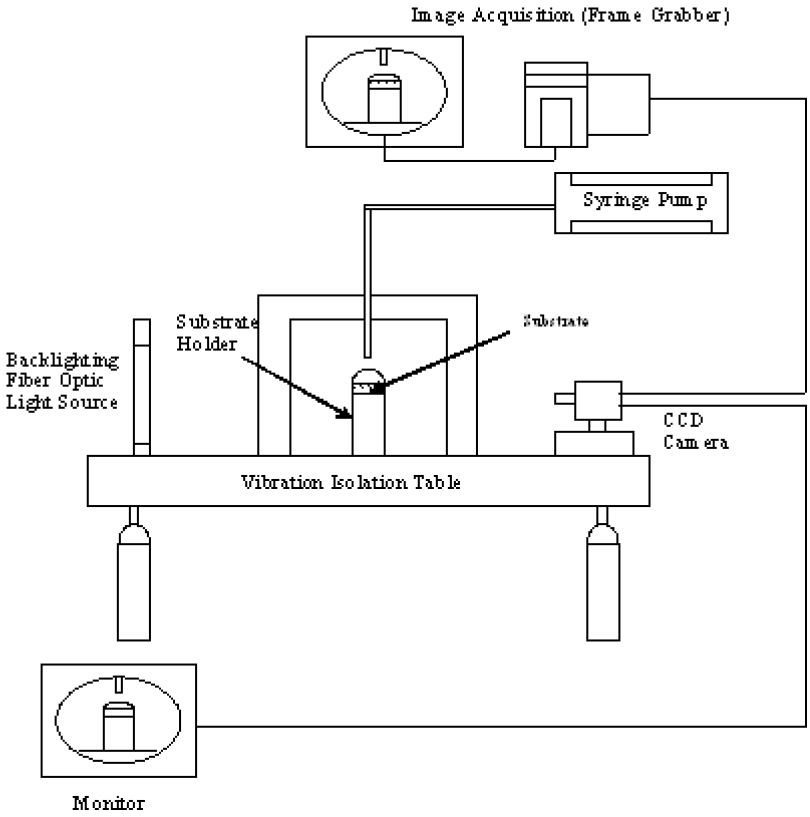

Fig. 2. Block diagram of the pendant and sessile drop apparatus for measuring interfacial tension and contact angle.

backlight (Edmund Optics K39-826) provides parallel lighting and is connected to a Dolan Jenner fiber optical illuminator (Model PL-900). The light source is supplied through the back of the environmental chamber. The camera is focused by optimizing the video image of a reticule (1×1 cm calibration area with 0.05×0.05 mm grid spacing). The reticule is located at the center plane of the drop. The grid reticule is an excellent detector of any image barreling and any other distortions inherent in the optics. It also provides the calibration factor for the horizontal and vertical magnification factors that are inherent in the camera and the optical systems. After digitizing the drop image, the gray levels for the pixel coordinates are found using the *Edge Tracking* function of Sigma Scan Pro 4.0 (Jandel Scientific Inc.). The image analysis software and the routines for the interfacial tension calculation are written in Fortran. All computations are executed on a Pentium 4 IBM personal computer.

3.3. Parameter estimation

The PSDA-FEM algorithm adjusts four parameter estimates to determine the surface tension (γ) and contact angle (θ_c) from sessile drop profiles. The γ-PD-FEM has been discussed earlier [26] and is based on a fixed contact line boundary condition. PSDA-FEM solves the Young–Laplace equation with a fixed contact angle boundary condition, or application of Young's equation for the surface energetics shown in Eq. (1). Ultimately, the four parameter estimates are G, x_0, θ_c, and y_0, while the volume is held constant during the iteration scheme. The constant volume constraint defines the reference pressure, K, and it is not a parameter estimate in the PSDA-FEM algorithm. The PSDA-FEM algorithm differs from the γ-PD-FEM algorithm because γ-PD-FEM algorithm uses K as a fitting parameter and the volume is allowed to adjust during the nonlinear regression subroutine. Initially, PSDA-FEM uses three parameter estimates (G, x_0, and θ_c) to ensure convergence and to allow close agreement between the theoretical and experimental drop shape coordinates. The value of y_0, defined at the apex, is added after an initial tolerance is achieved so that there are four parameter estimates (G, x_0, θ_c, and y_0) used to minimize the objective function (E_{FEM}) which is given as

$$\begin{aligned} E_{\mathrm{FEM},n} &= \left(f_n^{\mathrm{E}} - f_n^{\mathrm{T}}\right)^2 \\ &= \Big\{\left[\left(x_{\mathrm{T},n}^2 + y_{\mathrm{T},n}^2\right)\right] \\ &\quad - 2\sqrt{x_{\mathrm{T},n}^2 + y_{\mathrm{T},n}^2}\sqrt{\left(x_{\mathrm{E},n}^*\right)^2 + \left(y_{\mathrm{E},n}^*\right)^2} \\ &\quad + \left[\left(x_{\mathrm{E},n}^*\right)^2 + \left(y_{\mathrm{E},n}^*\right)^2\right]\Big\}, \quad n = 1, N. \end{aligned} \tag{10}$$

The proposed model seeks to minimize the square of the difference between the experimental (f^{E}) and theoretical (f^{T}) shape functions expressed in terms of the x and y coordinates as $(x_i^2 + y_i^2)^{1/2}$. Equation (10) is an expression for the objective function in terms of the experimental ($x_{\mathrm{E},n}$, $y_{\mathrm{E},n}$) and the theoretical ($x_{\mathrm{T},n}$, $y_{\mathrm{T},n}$) drop profile

coordinates, where $x^*_{E,n} = x_{E,n} - x_0$ and $y^*_{E,n} = y_{E,n} - y_0$ are defined for the adjusted experimental coordinates. The theoretical value of the shape function, f_n^T, is computed by a linear interpolation between the nodes ($f^T(\theta_i) = f_i^T$, $f^T(\theta_{i+1}) = f_{i+1}^T$), where $\theta_i \leqslant \theta_n \leqslant \theta_{i+1}$ and θ_n is the angle of the experimental shape function f_n^E. The difference (or distance) between the experimental and theoretical surface function values is not greatly affected by the flattening at the drop apex, because the surface function is defined in terms of the horizontal and vertical coordinates. Therefore, the bias usually observed for objective functions that are not based on the normal distance between an experimental data point and the theoretical curve is eliminated. This has been confirmed in [26].

An initial estimate for θ_c is obtained by linear regression on two or three experimental drop profile coordinates near the contact line depending on the total number of experimental coordinates. The value is calculated by setting the estimated slope of the line equal to $\tan(\theta_c)$. The initial value for θ_c is used during the initial three-parameter fit. After an initial convergence, y_0 is included in the four-parameter fit as described above. The parameters are updated and sent to the FEM subroutine to generate a theoretical drop shape.

4. Results and discussion

An algorithm with a fixed contact angle boundary condition (PSDA-FEM) is used to determine the interfacial tension (γ) and contact angle (θ_c) of simulated sessile drop profiles (Section 4.1) and simulated drop profiles with the equivalent of ±0.013, ±0.0065, and ±0.0033 mm randomized error (Section 4.2). The error in drop edge detection for a CCD camera with a resolution of 764 H × 494 V and the magnification of our experimental setup falls between ±0.0065 and ±0.013 mm. Simulated drop shapes with added randomized error equivalent to ±0.013, ±0.0065, and ±0.0033 mm are used with physical parameters that are close to those of the experimental drops. The estimates of γ and θ_c ($\hat{\gamma}$ and $\hat{\theta}_c$) for Mazola corn oil and water sessile droplets on an acrylic tape are also determined using PSDA-FEM. The expected accuracy of the output values using PSDA-FEM algorithm for these experimental systems is discussed in Section 4.2. The effect that the image resolution has on the accuracy and precision of $\hat{\gamma}$ for simulated sessile drop profiles with randomized error is presented in Section 4.3. The experimental results are discussed in Section 4.4. The results from the simulated data and experimental data confirm the validity of PSDA-FEM for obtaining interfacial tension and contact angle measurements from sessile drop profiles.

4.1. Simulated sessile drop profiles

The convergence **(**versatility**)** and accuracy of the PSDA-FEM algorithm is shown by using simulated sessile drop profiles which have contact angles less than 90°, equal to 90°, or greater than 90° at various drop volumes (Vol) and gravitational Bond numbers (G). Simulated sessile drop profiles are generated using the FEM at dimensional volumes similar to that of the experimental drops. The three volumes tested are 6.0, 10.0, and 20.0 mm^3 and contact angle values of 30.0°, 90.0°, and 110.0°. The range of Bond number values is 0.1 to 0.5 which results in interfacial tension ($\hat{\gamma}$) values that are comparable to the experimental results in Section 4.4. The interfacial tension is calculated by substituting 9.987×10^{-4} g/mm^3 for the density difference of water in air, 9987 mm/s^2 for the gravitational constant g, and the radius of the drop (mm) at the contact line into the expression for the gravitational Bond number given in Eq. (3). Table 1 is a summary of the results for three different drop shapes. The standard deviation in the parameter estimates is calculated for an average of twenty-four simulated runs. The standard deviation for $\hat{G}$ is ±0.001, and the deviations for Vol_{calc} and $\hat{\theta}_c$ are ±0.01 mm^3 and ±0.1°, respectively. The error between the parameter estimates $\hat{G}$ and $\hat{\theta}_c$ for the simulated drop shapes without randomized error is less than 0.03%, and the volume has an error of less than 1%. The % error in the average parameter estimates ($\hat{G}$, Vol_{calc}, $\hat{\theta}_c$, and $\hat{\gamma}$) at the three volumes has been measured at three different G values, and the general trend is the same for the % error in $\hat{G}$ and $\hat{\theta}_c$ at the three volumes. Therefore, one Bond number value at each volume is presented in Table 1, and the same simulated drop shapes are discussed further in the next section with added randomized error.

Table 1
% Error in parameter estimates for theoretical drop shapes with $\theta_c = 30.0°$, 90.0°, and 110.0° at Vol = 6.0, 10.0, and 20.0 mm^3

Bond number[a]			Volume[b] (mm^3)		Contact angle[c]	
Actual G	$\hat{G}$	% Error	Vol_{calc}	% Error	$\hat{\theta}_c$	% Error
0.500	0.500	0.0	5.97	0.50	29.9	0.00
0.130	0.130	0.0	10.0	0.02	89.8	0.01
0.100	0.100	0.0	20.0	0.02	109.8	0.01

[a] The standard deviation for $\hat{G}$ values is ±0.001.
[b] The standard deviation for Vol_{calc} values is ±0.01 mm^3.
[c] The standard deviation for $\hat{\theta}_c$ values is ±0.1°.

4.2. Simulated sessile drop shapes with randomized error

Randomized errors equivalent to ±0.013, ±0.0065, and ±0.0033 mm are added to the simulated drop profile coordinates discussed in Section 4.1. The random number function, Rand( ), in Fortran is used to add the equivalent randomized error to the theoretical drop profile data in order to simulate experimental data. Since the error added to the drop profile data pairs is different for each simulated data set, the random number generator can cause as much as a 15% difference in $\hat{\gamma}$ when the estimates of γ for eight simulated drop profiles with the same amount of randomized error are averaged. The average % error decreases as the number of data sets increases from eight to twenty-four, and approaches a global mean and standard deviation at twenty-four runs. Therefore,

Table 2
% Error in parameter estimates for simulated drop shapes with added randomized error[a,b,c] $\theta_c = 30.0°$, 90.0°, and 110.0° at Vol = 6.0, 10.0, and 20.0 mm^3, where $\Delta\rho = 9.987 \times 10^{-4}$ g/mm^3

Bond number			Volume (mm^3)		Contact angle		Interfacial tension (dyn/cm)		
Actual G	$\hat{G}$	% Error	Vol_{calc}	% Error	$\hat{\theta}_c$	% Error	γ_{actual}	$\hat{\gamma}_{\text{avg}}$	% Error
0.500	0.494 ± 0.034[a]	1.1	5.96 ± 0.04	0.63	29.9 ± 0.3	0.33	18.09	17.95 ± 1.15	0.77
0.130	0.134 ± 0.004[c]	2.9	10.01 ± 0.04	0.12	90.2 ± 0.2	0.23	69.55	68.22 ± 3.30	1.91
0.100	0.102 ± 0.001[b]	1.5	20.0 ± 0.1	0.13	110.0 ± 0.2	0.02	90.49	89.11 ± 1.78	1.42

[a] ±0.0033 mm randomized pixel error.
[b] ±0.0065 mm randomized pixel error.
[c] ±0.013 mm randomized pixel error.

a total of twenty-four simulated data sets at the three randomized unit length error values are chosen for this study due to the fact that the error in $\hat{\gamma}$ does not change by more than 1% from 24 to 30 runs. This is also chosen to closely simulate an actual experimental run with a reasonable number of trials.

The accuracy of the Sigma Scan Pro 4.0 edge detection software combined with the standard CCD camera used in this research falls between the results for ±0.0065 and ±0.013 mm randomized error. As the added error decreases, this is comparable to using a higher resolution camera or more advanced edge detection software. Table 2 summarizes the % error in the output parameter estimates $\hat{G}$, Vol_{calc}, $\hat{\theta}_c$, and $\hat{\gamma}$ that are averaged using twenty-four simulated runs of sessile drop shapes with added randomized errors. The surface tension values were computed from G as described in the previous section. The drop shapes were chosen because they resemble the experimental data discussed in Section 4.4 and to demonstrate the accuracy of the algorithm at low and high contact angles with various volumes and G values. The % error in Vol_{calc}, or the relative difference between the actual theoretical volume and calculated volume, remains less than 1%, and the % error in $\hat{\theta}_c$ is less than 0.5% for simulated drop shapes at all randomized error values. However, the % error in $\hat{G}$ and $\hat{\gamma}$ is 1.5% and 1.4%, respectively, for a Vol = 20.0 mm^3, $G = 0.100$, and $\theta_c = 110°$ with ±0.0065 mm added randomized error. The highest % error in $\hat{G}$ and $\hat{\gamma}$ at 2.9% and 1.9% is observed for a Vol = 10.0 mm^3, $\theta_c = 90.0°$, and ±0.013 mm added error. The simulated drop with Vol = 6.0 mm^3, $G = 0.500$, and $\theta_c = 30°$ has the least amount of error in $\hat{G}$ and $\hat{\gamma}$ at 1.1% and 0.77% because this drop shape has a ±0.0033 mm added randomized error. The effect the randomized error has on the accuracy of $\hat{\gamma}$ values is discussed further in Section 4.3, and will confirm that the errors in $\hat{G}$ and $\hat{\gamma}$ are within the expected accuracy of the PSDA-FEM algorithm at the corresponding contact angle and volume.

The drop shapes at three volumes are presented to show a graphical representation of the drop shapes and the random scatter of the residuals. Fig. 3 is a plot of the theoretical and simulated drop profiles with ±0.0033 mm added randomized error for Vol = 6.0 mm^3, $\theta_c = 30.0°$, and $G_{\text{actual}} = 0.500$. The surface function residual plot is shown in Fig. 4, the random scatter in Fig. 4 is typical for the drop profiles presented in this work. Fig. 5 is the drop profile with ±0.013 mm added randomized error for a drop with Vol = 10.0 mm^3, $\theta_c = 90.0°$, and $G_{\text{actual}} = 0.130$. Fig. 6 is a plot of the drop profiles with ±0.0065 mm added randomized error

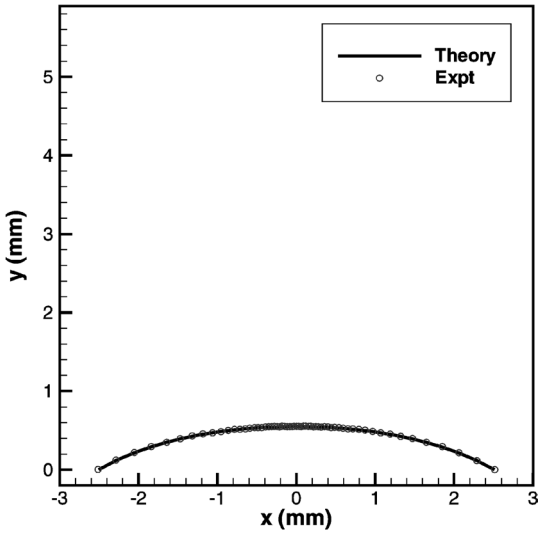

Fig. 3. Theoretical and simulated drop profiles with ±0.0033 mm added randomized error for Vol = 6.0 mm^3, $\theta_c = 30.0°$, where $G_{\text{actual}} = 0.500$ and $\hat{G} = 0.494 \pm 0.034$ using PSDA-FEM.

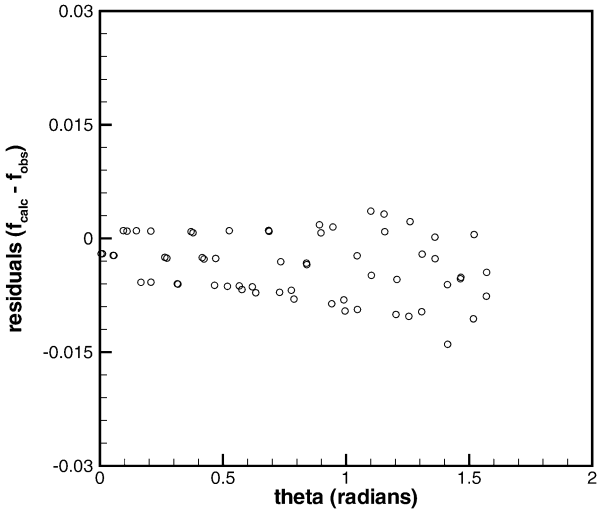

Fig. 4. Surface function residual plot for Fig. 3, where $G_{\text{actual}} = 0.500$, Vol = 6.0 mm^3, and $\theta_c = 30.0°$ using PSDA-FEM.

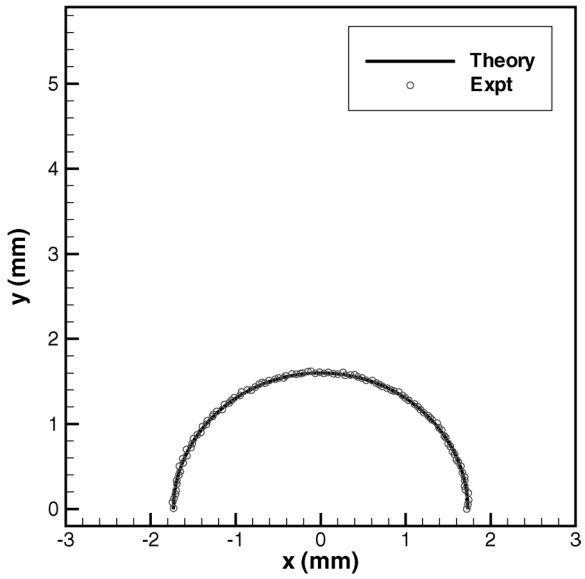

Fig. 5. Theoretical and simulated drop profiles with ±0.013 mm added randomized error for Vol = 10.0 mm^3, $\theta_c = 90.0°$, where $G_{actual} = 0.130$ and $\hat{G} = 0.134 \pm 0.004$ using PSDA-FEM.

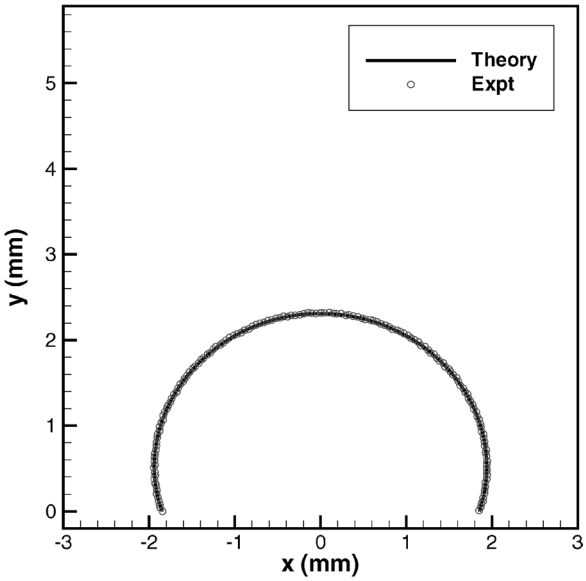

Fig. 6. Theoretical and simulated drop profiles with ±0.0065 mm added randomized error for Vol = 20.0 mm^3, $\theta_c = 110.0°$, where $G_{actual} = 0.100$ and $\hat{G} = 0.102 \pm 0.001$ using PSDA-FEM.

for Vol = 20.0 mm^3, $\theta_c = 110.0°$, and $G_{actual} = 0.100$. In all cases, the residual plots show random scatter about zero that is similar to the data in Fig. 4. A study on the error of output γ values at four θ_c values for all three randomized error values is discussed further in Section 4.3.

4.3. Effect of pixel size on the accuracy and precision of $\hat{\gamma}$ (dyne/cm) at various angles

The effect of image resolution on the parameter estimates using PSDA-FEM is examined by obtaining $\hat{\gamma}$ values for

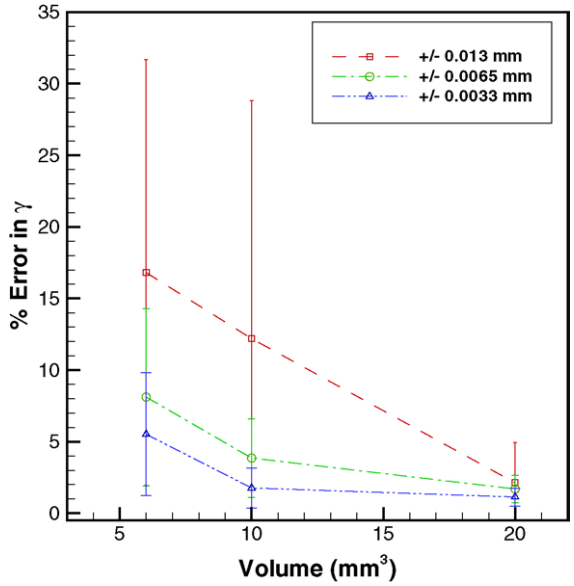

Fig. 7. The average % error in $\hat{\gamma}$ values for simulated sessile drops with $\theta_c = 30.0°$ and added randomized error (mm) at Vol = 6.0, 10.0, and 20.0 mm^3.

simulated drop shapes with Vol = 6.0, 10.0, and 20.0 mm^3. Randomized errors (or simulated pixel sizes) of ±0.013, ±0.0065, and ±0.0033 mm were added to the drop profile coordinates. The Vol_{calc} and $\hat{\theta}_c$ differ by less than 1% of actual simulated drop shape input variables for simulations performed at all three randomized error values. Therefore, the results are presented for the % error in $\hat{\gamma}$ to show the relative error expected in the experimental values obtained using PSDA-FEM. It has been noted in the literature [16–23] that the sessile drop technique does not have the same accuracy in interfacial tension measurements as the pendant drop technique due to asymmetry and nonuniformity of the substrate surface. In addition to these sources of error, it is also necessary to evaluate the effect of pixel size on the accuracy and precision of the parameter estimates for γ. The accuracy is defined in terms of the % error or difference between the average parameter estimates of γ for several simulated drop profiles with randomized error and the actual value of γ. The precision of the parameter estimate of γ is obtained by determining the % deviation (standard deviation) about the mean of parameter estimates of γ from multiple data sets where randomized error has been added to the same original simulated drop profile without randomized error.

The accuracy in output γ values is shown as a plot of the average % error as a function of the volume (mm^3). The error bars represent the standard deviation of the error obtained for $\hat{\gamma}$ in twenty-four simulated runs. Figs. 7, 8, and 9 are plots of the average % error in $\hat{\gamma}$ as a function of volume at 6.0, 10.0, and 20.0 mm^3 and the three simulated pixel sizes of ±0.013, ±0.0065, ±0.0033 mm for $\theta_c = 30°$, 90°, and 110°. The average % error in the $\hat{\gamma}$ value decreases from less than 10 to 3% as the volume increases from 6.0 to 20.0 mm^3 at ±0.013 mm randomized error for 30°, 90°, and 110° (Figs. 7, 8, and 9). The error in $\hat{\gamma}$ decreases from 15 to

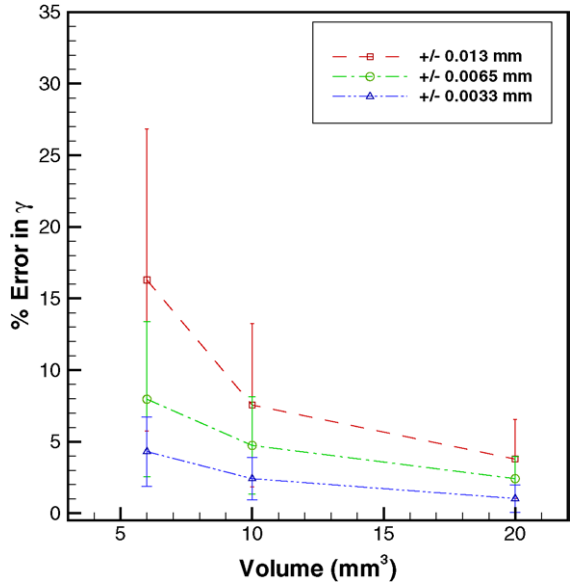

Fig. 8. The average % error in $\hat{\gamma}$ values for simulated sessile drops with $\theta_c = 90.0°$ and added randomized error (mm) at Vol = 6.0, 10.0, and 20.0 mm^3.

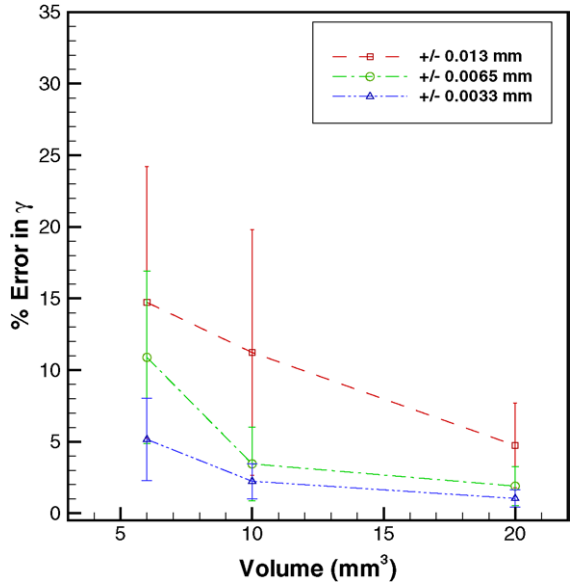

Fig. 9. The average % error in $\hat{\gamma}$ values for simulated sessile drops with $\theta_c = 110.0°$ and added randomized error (mm) at Vol = 6.0, 10.0, and 20.0 mm^3.

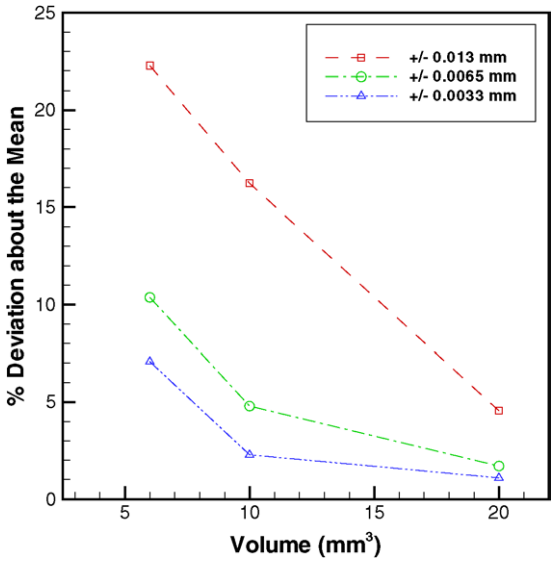

Fig. 10. The precision of $\hat{\gamma}$ values for simulated sessile drops with $\theta_c = 30.0°$ and added randomized error (mm) at Vol = 6.0, 10.0, and 20.0 mm^3.

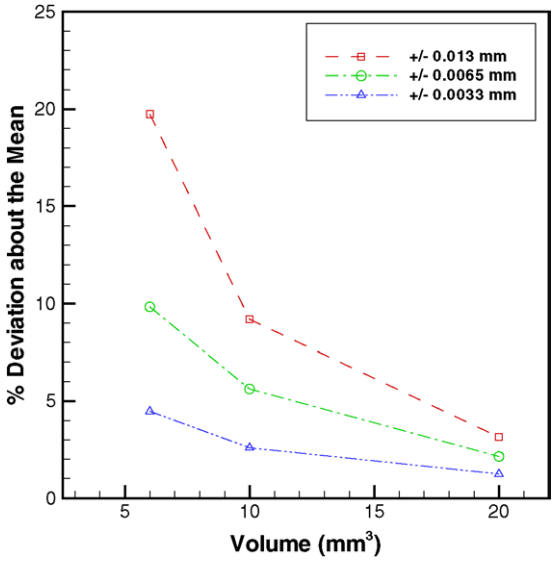

Fig. 11. The precision of $\hat{\gamma}$ values for simulated sessile drops with $\theta_c = 90.0°$ and added randomized error (mm) at Vol = 6.0, 10.0, and 20.0 mm^3.

5% with a decrease in the simulated pixel size from ±0.013 to ±0.0033 mm for Vol = 6.0 mm^3, or a small drop volume, at the three contact angles.

The standard deviation of the error decreases as the resolution improves or the simulated pixel size decreases from ±0.013 to ±0.0033 mm and as the drop volume increases. This data shows that a high resolution camera coupled with experimental drop volumes greater than 10.0 mm^3 results in more accurate experimental $\hat{\gamma}$ values. As an example, a drop volume of 6.0 mm^3 and $\theta_c = 30°$ with ±0.0033 mm randomized error has an expected error in $\hat{\gamma}$ between 1 and 10%.

The precision of the PDSA-FEM technique is also measured for twenty-four simulated experimental runs. The % deviation about the mean as a function of the volume at three contact angles (30°, 90°, and 110°) is summarized for three added randomized errors (±0.013, ±0.0065, and ±0.0033 mm). Figs. 10, 11, and 12 show that overall the precision of the measurement improves with increased volume and decrease in pixel size. The largest % deviation about the mean, or the smallest precision in $\hat{\gamma}$, is 20% for Vol = 6.0 mm^3 at $\theta_c = 30.0°$ and 90.0° for drop profiles with ±0.013 mm added randomized error. The % deviation

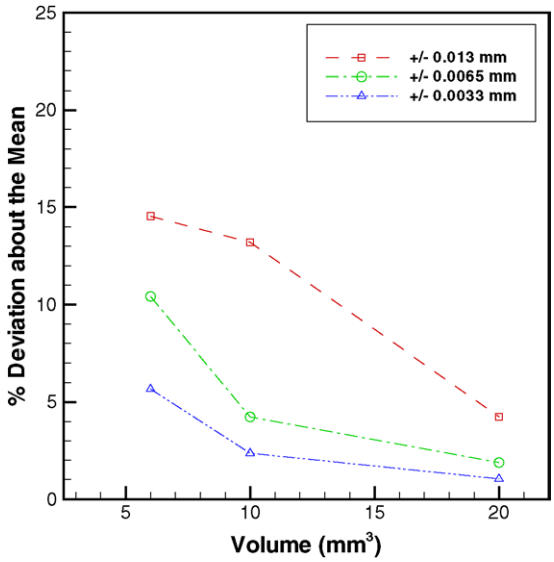

Fig. 12. The precision of $\hat{\gamma}$ values for simulated sessile drops with $\theta_c = 110.0°$ and added randomized error at Vol = 6.0, 10.0, and 20.0 mm^3.

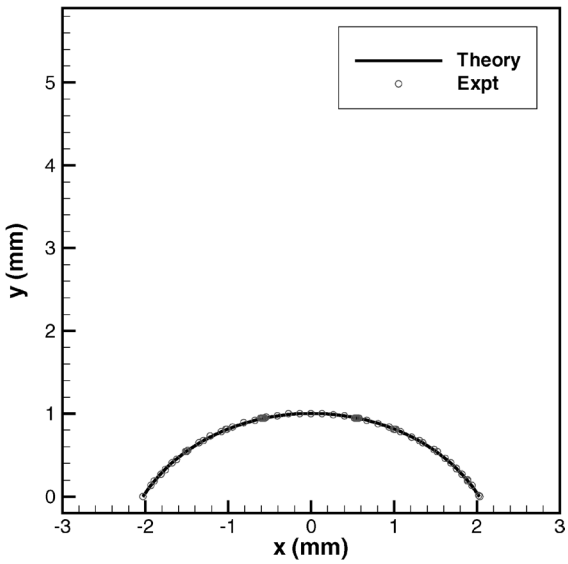

Fig. 13. Experimental and theoretical drop profiles for experimental Mazola corn oil drop on acrylic tape at 22 °C where $\hat{\theta}_c = 56.0° \pm 1.5°$, $\hat{\gamma} = 70.2 \pm 0.5$ dyn/cm using PSDA-FEM.

decreases to a minimum of 5% with a decrease in the randomized unit error at this smaller volume. The precision of the measurements at 110° has an initial value of 15% at Vol = 6.0 mm^3 for ±0.013 mm and decreases to 5% for ±0.0033 mm randomized error. The precision in $\hat{\gamma}$ at Vol = 10.0 mm^3 is an average of 10% at ±0.013 mm pixel size and improves to 5% for the highest resolution (pixel size ±0.0033 mm) at all three contact angles. The % deviation about the mean for Vol = 20.0 mm^3 is an average of 10% at the largest pixel size (±0.013 mm) and improves to 1% with a pixel size of ±0.0033 mm at all three contact angles. Therefore, the expected average % error in γ and % deviation about the mean should fall within the 5–10% range for surface tension values that are obtained using experimental sessile drop profiles that are imaged using the CCD camera and optical equipment described in Section 3.2.

4.4. Experimental drop shape results

The ability of the PSDA-FEM algorithm to obtain experimental interfacial tension values and contact angle measurements is demonstrated using two liquid systems. Mazola corn oil (cooking oil) and water droplets are formed on acrylic tape substrates. The theoretical and experimental drop profiles for oil on acrylic are shown in Fig. 13 and the surface function residual plot is randomly scattered about zero (not shown). The average interfacial tension value obtained for six drops is 30.0 ± 1.1 dyn/cm, and the contact angle is 56.0° ± 1.5°. This value of interfacial tension agrees within 6% of the value obtained for the average interfacial tension value for four drops of 31.9 ± 0.23 dyn/cm determined by the pendant drop technique (γ-PD-FEM). The 6% error obtained for the Mazola corn oil on acrylic is within the % error limits of the simulations performed using ±0.0065 mm randomized error. Furthermore, the error and standard deviation for our parameter estimates of the interfacial tension are similar to or even better than those reported by Emelyanenko and Boinovich [23]. They reported interfacial tension estimates with >10% standard deviation about the mean and errors of approximately 6% for sessile drops with contact angles around 56°. Emelyanenko and Boinovich [23] also showed how the precision and accuracy of the measurements improved with an increase in the contact angle. The volume of the experimental drops varied from 6.0 to 15.0 mm^3 which is in the range of the simulated drop volumes. The less than 2% deviation for the average contact angle provides confidence in accuracy of measured contact angle by using this technique.

The experimental and theoretical drop profiles for water on acrylic tape are shown in Fig. 14. The average interfacial tension value for three water droplets is 65.9 ± 5.0 dyn/cm and the average contact angle 95.6° ± 2.0°. This γ value is 8% different than reported literature values for pure water (72.0 dyn/cm) and reflects the sensitivity of the interfacial tension of water to trace surface active impurities. The γ and θ_c value for water on acrylic shows that the PSDA-FEM algorithm can solve for contact angles less than or greater than 90°. The surface function residual plot (not shown) has random scatter about the central axis confirming that the drop is axisymmetric (at least in the plane of the image) and that the model assumptions are valid.

The sessile drop analysis algorithm (PSDA-FEM) determines simultaneously $\hat{\gamma}$ and $\hat{\theta}_c$ from digital drop profiles. This allows for the measurement of the effective surface tension and contact angle for liquids on substrates covered with surface active molecules, macromolecules and colloids where the “real-time” determination of the properties of the liquid and its interaction with the substrate material are important.

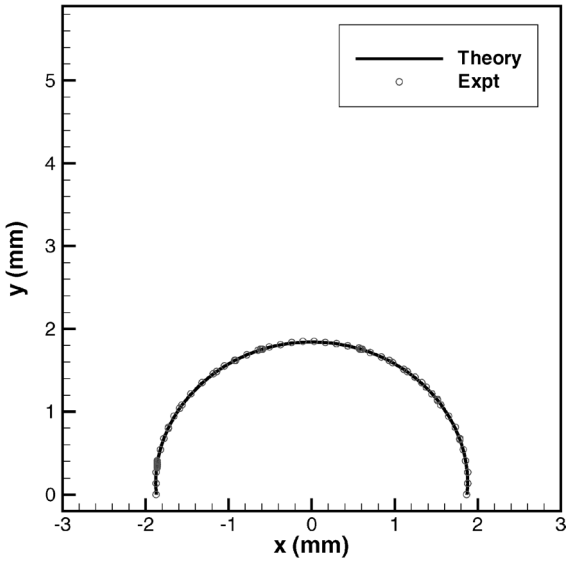

Fig. 14. Experimental and theoretical drop profiles for experimental water sessile drop on acrylic tape at 22 °C where $\hat{\theta}_c = 95.6° \pm 2.0°$, $\hat{\gamma} = 30.0 \pm 1.1$ dyn/cm using PSDA-FEM.

5. Conclusion

A computational method has been previously discussed to determine the interfacial tension of pendant drops using a finite-element-based algorithm (γ-PD-FEM) and the results are compared to arc-length-based algorithms using the Bashforth–Adams equations. However, the ability to measure both θ_c and γ of a liquid/solid system is a major benefit of the sessile drop technique. This paper presents a modified algorithm which allows simultaneous determination of the interfacial tension and contact angle from sessile drop profiles (PSDA-FEM). The PSDA-FEM algorithm has been tested using theoretical and simulated drop shapes to estimate the effect of pixel size (camera resolution) and sessile drop volume on the accuracy and precision of the surface tension values. The surface tension estimates for two experimental systems (water on acrylic and cooking oil on acrylic) are within the predicted ranges for accuracy and precision. Despite the slightly larger error in γ obtained using the sessile drop technique, the PSDA-FEM is useful for studying systems where the surface tension of the liquid changes with time due to the transfer of surface active agents from the substrate to the liquid medium. Conventional methods usually require a separate measurement such as the pendant drop or Dunouy ring method to obtain a value for γ; however, this will not capture the solid–liquid interaction that may occur during sessile drop measurements. The PSDA-FEM algorithm is able to characterize this phenomenon by the incorporation of both physical boundary conditions at the apex and drop contact line into the problem formulation.

Acknowledgments

The authors thank Dr. Osman A. Basaran, Chemical Engineering Department at Purdue University, for his teaching and advice on development of the finite element method subroutine. We thank Kristianto Tjiptowidjojo for collaborating on the design and manufacture of the temperature-controlled chamber. This work was funded by the Gates Millennium Scholarship, the Ford Pre-Doctoral Fellowship, the GEM Ph.D. Fellowship, the National Science Foundation (DMR-9700860), and the Department of Energy (DE-FG02-02ER45976).

References

[1] J. Bachmann, A. Ellies, K.H. Hartge, J. Hydrol. 231 (2000) 66.
[2] B.J. Carroll, J. Adhes. Sci. Technol. 6 (1992) 983.
[3] P.D. Ownby, J. Liu, J. Adhes. Sci. Technol. 2 (1988) 255.
[4] E.I. Vargha-Butler, S.J. Sveinsson, Z. Policova, Colloids Surf. 58 (1991) 271.
[5] E.I. Vargha-Butler, E. Kiss, C.N.C. Lam, Z. Keresztes, E. Kalman, L. Zhang, A.W. Neumann, Colloid Polym. Sci. 279 (2001) 1160.
[6] N. Kaiser, A. Croll, F.R. Szofran, S.D. Cobb, K.W. Benz, J. Cryst. Growth 231 (2001) 448.
[7] H.J. Busscher, W. Vandervegt, J. Noordmans, J.M. Schakenraad, H.C. Vandermei, Colloids Surf. 58 (1991) 229.
[8] R.Y. Tsay, S.C. Yan, S.Y. Lin, Rev. Sci. Instrum. 66 (1995) 5065.
[9] E. Rame, J. Colloid Interface Sci. 185 (1997) 245.
[10] Y.G. Gu, D.Q. Li, P. Cheng, Colloids Surf. A Physicochem. Eng. Aspects 122 (1997) 135.
[11] A.M. Emelyanenko, N.V. Ermolenko, L.B. Boinovich, Colloids Surf. A Physicochem. Eng. Aspects 239 (2004) 25.
[12] A. Bateni, S.S. Susnar, A. Amirfazli, A.W. Neumann, Colloids Surf. A Physicochem. Eng. Aspects 219 (2003) 215.
[13] J.S. Allen, J. Colloid Interface Sci. 261 (2003) 481.
[14] M.W. Yang, S.Y. Lin, Colloids Surf. A Physicochem. Eng. Aspects 220 (2003) 199.
[15] J. Chatterjee, J. Colloid Interface Sci. 259 (2003) 139.
[16] F.K. Hansen, J. Colloid Interface Sci. 160 (1993) 209.
[17] A.M. Emelyanenko, L.B. Boinovich, Instrum. Exp. Tech. 45 (2002) 44.
[18] D. Li, P. Cheng, A.W. Neumann, Adv. Colloid Interface Sci. 39 (1992) 347.
[19] J.D. Malcolm, H.M. Paynter, J. Colloid Interface Sci. 82 (1981) 269.
[20] F.K. Skinner, Y. Rotenberg, A.W. Neumann, J. Colloid Interface Sci. 130 (1989) 25.
[21] E. Moy, P. Cheng, Z. Policova, S. Treppo, D. Kwok, R.D. Mack, P.M. Sherman, A.W. Neumann, Colloids Surf. 58 (1991) 215.
[22] C. Huh, R.L. Reed, J. Colloid Interface Sci. 91 (1983) 472.
[23] A.M. Emelyanenko, L.B. Boinovich, Colloids Surf. A Physicochem. Eng. Aspects 189 (2001) 197.
[24] M.G. Cabezas, A. Bateni, J.M. Montanero, A.W. Neumann, Appl. Surf. Sci. 238 (2004) 480.
[25] O.I. del Rio, A.W. Neumann, J. Colloid Interface Sci. 196 (1997) 135.
[26] N.M. Dingle, K. Tjiptowidjojo, O.A. Basaran, M.T. Harris, J. Colloid Interface Sci. (2005), in press.
[27] O.I. del Rio, D.Y. Kwok, R. Wu, J.M. Alvarez, W.A. Neumann, Colloids Surf. A Physicochem. Eng. Aspects 143 (1998) 197.